

## REVIEW

[View Article Online](#)  
[View Journal](#) | [View Issue](#)Cite this: *RSC Med. Chem.*, 2025, 16, 1532

# Synthetic strategies and medicinal chemistry perspectives of dual acting carbonic anhydrase modulators with monoamine oxidase and cholinesterase inhibitors

Sandeep Bindra,<sup>ab</sup> Ehab M. Mostafa,<sup>id</sup>\*<sup>c</sup> Mohamed A. Abdelgawad,<sup>d</sup> Samy Selim,<sup>e</sup> Sunil Kumar<sup>b</sup> and Bijoy Mathew<sup>id</sup>\*<sup>b</sup>

Multi-target drug design (MTDD) represents the paradigm shift in pharmaceutical research, moving beyond the conventional one-drug-one-target approach to address the complexity of multifactorial diseases. This strategy aims to develop single therapeutic candidates that can simultaneously modulate multiple biological targets, offering more comprehensive disease management and reducing the likelihood of drug resistance. In this article, we highlighted the design, synthesis, and structure–activity relationships (SARs) of various dual acting inhibitors involved in treatment of neurodegenerative diseases. Dual acting inhibitors targeting carbonic anhydrases (CAs), monoamine oxidases (MAOs), and cholinesterases (ChEs) have emerged as promising therapeutic agents due to their potential in treating complex neurodegenerative and psychiatric disorders such as Alzheimer's disease (AD) and Parkinson's disease (PD). By integrating CA inhibitors with MAO and ChE inhibition, researchers aim to address both the neuroprotective and symptomatic aspects of these disorders. The review also discusses key SAR studies that have guided the optimization of dual inhibitors, focusing on achieving selectivity and potency while minimizing off-target effects. From a medicinal chemistry perspective, the dual inhibition approach offers advantages such as improved efficacy, reduced polypharmacy, and better management of disease progression. However, challenges remain, including maintaining selectivity for target isoforms and overcoming pharmacokinetic limitations. Overall, the development of dual-acting CA–MAO–ChE inhibitors represents a compelling avenue in drug discovery, with the potential to significantly impact the treatment of neurodegenerative diseases.

Received 26th October 2024,  
Accepted 18th January 2025

DOI: 10.1039/d4md00837e

[rsc.li/medchem](http://rsc.li/medchem)

## 1. Introduction

Multi-target drugs are therapeutic agents designed to act on multiple molecular targets or pathways simultaneously (Fig. 1). These drugs are becoming increasingly important in the treatment of complex diseases, particularly cancer, metabolic syndrome, neurodegenerative disorders, inflammation and infectious diseases.<sup>1</sup> Even if their discovery has long been due

to serendipity. Multiple additive or synergistic pharmacodynamic activities may be highly advantageous for treating certain disorders in terms of increased therapeutic efficacy or postponed development of resistance. There are several reasons why multitarget drugs are crucial: 1. complex diseases involve multiple pathways, 2. reduction of drug resistance, 3. synergistic effects, 4. improved patient compliance, and 5. reduced toxicity.<sup>2,3</sup>

### 1.1. Complex diseases involve multiple pathways

Many complex diseases like cancer, diabetes, and neurodegenerative diseases, involve a network of signaling pathway. A single-target drug may not be sufficient to manage such diseases effectively. Multitarget medications can achieve more thorough therapeutic effects by targeting multiple pathways. For instance, lapatinib (Fig. 2) is a reversible ATP-competitive inhibitor of the human epidermal growth factor receptor 2 (HER2), and breast cancer is treated by targeting epidermal growth factor receptor (EGFR) tyrosine kinases.<sup>4</sup>

<sup>a</sup> Dr. Bhagat Singh Rai College of Pharmacy, Mandla Road, Seoni-480661, Madhya Pradesh, India<sup>b</sup> Department of Pharmaceutical Chemistry, Amrita School of Pharmacy, Amrita Vishwa Vidyapeetham, Amrita Health Science Campus, Kochi-682041, Kerala, India. E-mail: [bijomathew@aims.amrita.edu](mailto:bijomathew@aims.amrita.edu), [bijovilaventgu@gmail.com](mailto:bijovilaventgu@gmail.com)<sup>c</sup> Department of Pharmacognosy, College of Pharmacy, Jouf University, Sakaka 72388, Saudi Arabia. E-mail: [emmoustafa@ju.edu.sa](mailto:emmoustafa@ju.edu.sa)<sup>d</sup> Department of Pharmaceutical Chemistry, College of Pharmacy, Jouf University, Sakaka 72388, Saudi Arabia<sup>e</sup> Department of Clinical Laboratory Sciences, College of Applied Medical Sciences, Jouf University, Sakaka, 72388, Saudi Arabia

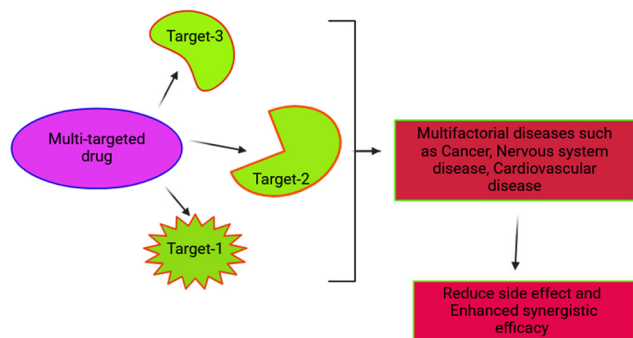


Fig. 1 Multi-target drug design.

## 1.2. Reduction of drug resistance

One of the main challenges in diseases like cancer and infections is the development of drug resistance. Single-target therapies can lead to the emergence of resistant strains or cells, as the disease can adapt to inhibit one target. Multitarget drugs reduce the likelihood of resistance by simultaneously attacking multiple vulnerabilities within a disease, making it harder for resistant variants to emerge. Antitubercular medication with multi-target characteristics, SQ109 (Fig. 2), for instance, has been shown to inhibit MenA and MenG, which are involved in the manufacture of menaquinones, as well as MmpL3 and MmpL11, which are transporter proteins involved in the formation of cell walls.<sup>5</sup>

## 1.3. Synergistic effect

Targeting multiple pathways or molecules can create a synergistic effect, where the combined effect of the drug on different targets is greater than the sum of its individual effects. This can improve the overall efficacy of the treatment and may allow for lower dosages, reducing side effects of drugs, such as caproctamine (Fig. 2), which showed a synergistic cholinergic action against Alzheimer's disease (AD) by antagonizing presynaptic muscarinic acetylcholine M2 autoreceptors and inhibiting acetylcholinesterase (AChE).<sup>6</sup>

## 1.4. Improved patient compliance

Multitarget drugs can potentially reduce the number of medications a patient has to take, simplifying treatment regimens. For instance, instead of taking multiple drugs to target different aspects of a disease, a single multitarget drug could achieve the same results. This can lead to better adherence to treatment.<sup>7</sup>

## 1.5. Reduced toxicity

By distributing the drug's effects across several targets rather than focusing on a single one at high potency, multitarget drugs may help minimize the risk of off-target effects and toxicity, leading to a better safety profile.<sup>8</sup> For example, sorafenib (Fig. 2) was approved by the FDA for the treatment of renal cell carcinoma (RCC) in 2005, unresectable hepatocellular carcinoma (HCC) in 2007 and radioiodine-refractory differentiated thyroid carcinoma in 2013.<sup>9–11</sup> Sorafenib inhibits the activity of serine-threonine kinases Raf-1 and B-Raf, vascular endothelial growth factor receptor (VEGFR)-1/2/3, platelet-derived growth factor receptor  $\beta$  (PDGFR- $\beta$ ), c-Kit, RET, and FLT3.<sup>12–14</sup>

Multi-target drug design for CNS acting molecules focuses on creating compounds that can interact with several biological targets implicated in CNS disorders. Conditions such as Alzheimer's disease, Parkinson's disease, depression, and schizophrenia involve intricate pathological mechanisms. By addressing multiple pathways at once, this approach offers potential therapeutic benefits, tackling the complex and multifactorial nature of these diseases more effectively.<sup>15</sup> In the development of multi-target drug design, dual-acting molecules play a crucial role. Dual-acting molecules for CNS disorders are drugs designed to target two distinct biological mechanisms such as monoamine oxidase (MAO) and acetylcholinesterase/butyrylcholinesterase (AChE/BChE), MAO and carbonic anhydrases (CAs)<sup>16</sup> or AChE/BChE and CAs, providing broader therapeutic effects. There are several dual-acting drug molecules in the last 5

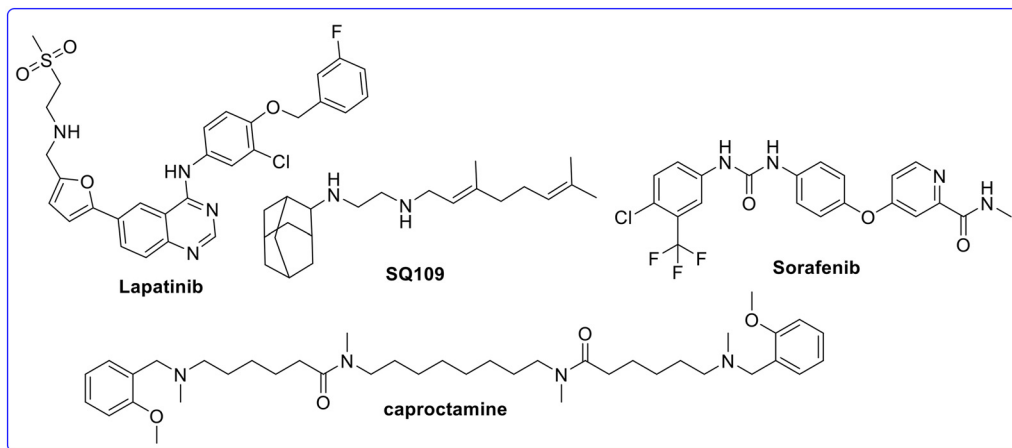


Fig. 2 Structures of clinically used multi-target drugs.

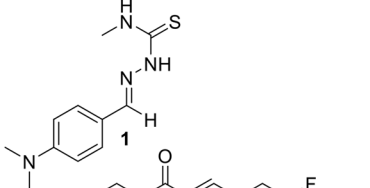
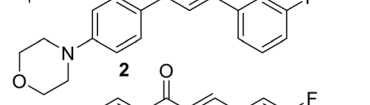
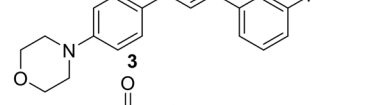
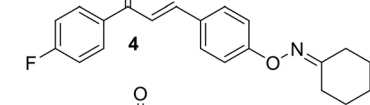
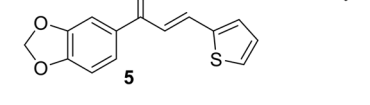
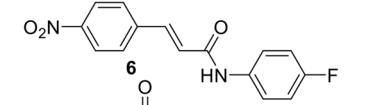
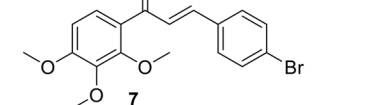
Com	MAO-A (IC <sub>50</sub> , μM)	MAO-B (IC <sub>50</sub> , μM)	AChE (IC <sub>50</sub> , μM)
	55.5	48.9	75.2
	45	0.087	>50
	>40	0.030	16.1
	4.0	0.018	>40
	0.023	0.026	9.57
	15.2	0.0092	8.02
	14.4	0.46	19.8
			BACE1 (IC <sub>50</sub> , μM)

Fig. 3 Dual acting drugs used in the treatment of neurological diseases.<sup>17–23</sup>

years for the treatment of CNS diseases, which are discussed below (Fig. 3).

Carbonic anhydrases (CAs) are a family of zinc metalloenzymes catalyzing the reversible reaction of CO<sub>2</sub> and H<sub>2</sub>O into bicarbonate ions and protons.<sup>24,25</sup> CAs are mainly found in archaea, prokaryotes, and eukaryotes. They are encoded by eight distinct, evolutionarily unrelated genes known as α-CAs (found in vertebrates, eubacteria, algae, and the cytoplasm of green plants), β-CAs (primarily in eubacteria, algae, and the chloroplasts of both monocots and dicots), and γ-CAs (mainly in archaea and some eubacteria), and δ-, η-, θ-, ζ- (found in marine diatom) and ι-CAs (found in diatoms and bacteria).<sup>26–30</sup> In mammals, 16 distinct α-CA isozymes or CA-related proteins (CARPs) have been identified, each exhibiting unique subcellular localization and tissue distribution.<sup>31–33</sup> Some of these CA isozymes are cytosolic, including CA I, CA II, CA III, CA VII, and CA XIII. Others are membrane-bound, such as CA IV, CA IX, CA XII, CA XIV, and CA XV. CA VA and CA VB are localized in the mitochondria, while CA VI is secreted in saliva and milk. Additionally, there are three known catalytic forms of the CA-related proteins (CARPs), specifically CARP VIII, CARP X, and CARP XI, which also appear to be cytosolic proteins.<sup>34</sup> These enzymes catalyze a simple yet vital physiological reaction: the interconversion between carbon dioxide and bicarbonate ions. This process plays a key role in several crucial physiological functions, including respiration

and the transport of CO<sub>2</sub>/bicarbonate between metabolizing tissues and the lungs, maintaining pH and CO<sub>2</sub> homeostasis, and facilitating electrolyte secretion in various tissues and organs. They are also involved in biosynthetic pathways like gluconeogenesis, lipogenesis, and ureagenesis, as well as in bone resorption, calcification, tumorigenesis, and many other physiological and pathological processes.<sup>35,36</sup> As will be discussed shortly, many of these isozymes are key targets for the design of inhibitors with potential clinical applications. In

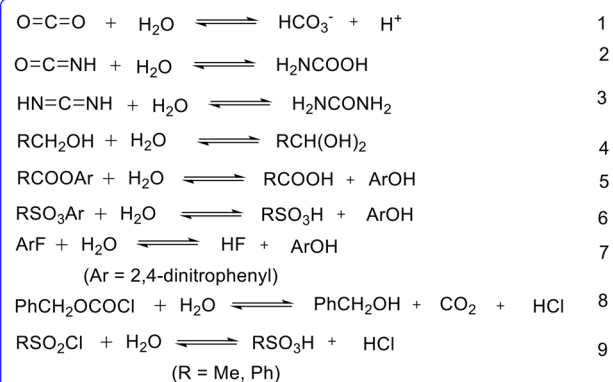


Fig. 4 Reactions catalyzed by α-carbonic anhydrase.

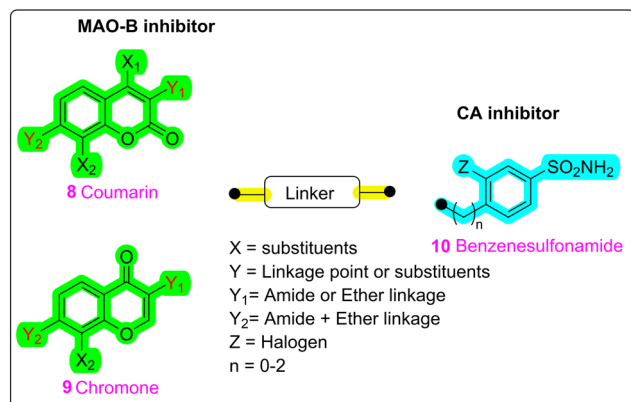


Fig. 5 Drug design strategy of dual acting inhibitors of CAs and MAO-B.

addition to catalyzing the reversible hydration of CO<sub>2</sub> to bicarbonate (reaction (1), Fig. 4), carbonic anhydrases also facilitate several other reactions. These include the hydration of cyanate to carbamic acid and cyanamide to urea (reactions (2) and (3)), the hydration of aldehydes to form *gem*-diols (reaction (4)), and the hydrolysis of carboxylic acids or sulfonic acids (reactions (5) and (6)). They are also involved in other, less-studied hydrolytic processes, as described in reactions (7)–(9).<sup>36,37</sup> The recent advancements in the development of CA inhibitors (CAIs) have led to the creation of novel therapeutic agents targeting a wide range of diseases. The new generations of CAIs are being designed with improved selectivity, potency, and pharmacokinetic properties, including sulfonamides, coumarins, and sulfamates.<sup>38,39</sup> CAIs are being explored due to their potential in treating conditions such as glaucoma, epilepsy, obesity, and cancer.<sup>40–45</sup> Additionally, CAIs are being investigated for their roles in managing conditions like hypertension, osteoporosis, and neurological disorders. In Alzheimer's disease (AD) and cerebral amyloid angiopathy (CAA), harmful amyloid-beta (Aβ) aggregates build up around and within the walls of cerebral vessels, and form parenchymal plaques in specific brain regions such as the hippocampus and cortex.<sup>46</sup> Researchers have shown that cytochrome c is released from the mitochondria of the neurovascular unit (NVU) in a variety of cell types, including endothelial cells (ECs), smooth muscle cells (SMCs), neurons, and glial cells, as a result of Aβ oligomers and protofibrils. Caspases are activated as a result of

this release, which causes cell death.<sup>47,48</sup> Methazolamide (MTZ) reduced mitochondria-mediated cell death caused by Aβ in all neurovascular cell types. Additionally, MTZ lowered the activation of caspase-3 and caspase-9 in endothelial cells, neurons, and glial cells *in vitro*, and also reduced caspase-3 activation *in vivo*.<sup>49</sup> Furthermore, in cerebrovascular endothelial cells, acetazolamide (ATZ) and MTZ inhibited Aβ-induced caspase-9 activation and subsequent apoptosis. Sun and Alkon demonstrated that CAAs improve synaptic efficacy, spatial learning, and memory in rats, as shown by the Morris water maze test. This effect occurs because CA activation increases bicarbonate (HCO<sub>3</sub><sup>−</sup>) levels in the hippocampus, which triggers a shift in GABAergic synaptic outputs from inhibitory to excitatory.<sup>50</sup> Under these conditions, GABA activates a specific group of hippocampal pyramidal neurons, thereby enhancing associative memory formation. In 2017, research found that CAA (D-phenyl alanine) improves object recognition memory in mice by promoting ERK phosphorylation in the cortex and hippocampus.<sup>51</sup> Cytosolic carbonic anhydrases, particularly isoforms II and VII, are thought to be the primary isozymes responsible for this pharmacological effect.<sup>52</sup>

Monoamine oxidase (MAO) is a mitochondrial, flavin-dependent enzyme responsible for metabolizing arylalkylamine neurotransmitters such as epinephrine, norepinephrine (NE), dopamine (DA), serotonin (5-HT), and phenylethylamine (PEA), along with various exogenous amines. This process occurs through oxidative deamination, converting these compounds into their corresponding aldehydes and hydrogen peroxide (H<sub>2</sub>O<sub>2</sub>) in the central nervous system (CNS) and tissues.<sup>53</sup> The Fenton reaction, catalyzed by iron and neuromelanin, transforms hydrogen peroxide (H<sub>2</sub>O<sub>2</sub>) into highly dangerous reactive oxygen species (ROS).<sup>54</sup> Two isoforms of MAO, known as MAO-A and MAO-B, have been identified based on differences in enzyme inhibition, substrate selectivity, specificity, amino acid sequence, and tissue distribution.<sup>55</sup> The enzyme MAO-A preferentially deaminates neurotransmitters such as serotonin, adrenaline, and noradrenaline (*e.g.*, inhibited by clorgyline), while MAO-B primarily oxidizes phenylethylamine and benzylamine (*e.g.*, inhibited by selegiline). Both isoforms, however, are active against tyramine and dopamine.<sup>56</sup> The primary differences between MAO-A and MAO-B lie in the specific details of their active sites, which explain their varying substrate and inhibitor selectivities.

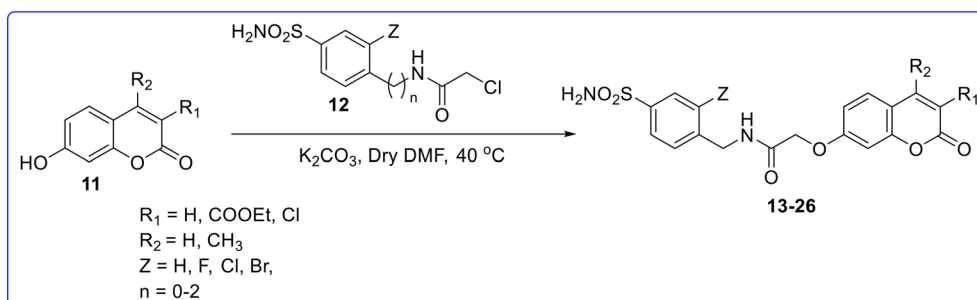


Fig. 6 Synthesis of compounds 13–26.

Com	Z	n	R1	R2	
13	H	2	COOEt	H	H ↑ Highest CAs inhibitory activity against CA II, VA, VII ( $K_i$ value = 0.8 to 9.4 nM)
14	F	0	H	H	H → Good inhibitory activity against CA II, VA, VB, VII ( $K_i$ value = 8.9 to 25.5 nM)
				AAZ	→ $K_i$ value = 2.5 to 63 nM
				MTZ	→ $K_i$ value = 2.1 to 65 nM
15	F	0	COOEt	H	} Retain CAs inhibitory activity
16	Br	0	COOEt	H	
17	H	0	COOEt	H	
18	H	0	H	H	} CAs inhibitory activity decreases
19	Cl	0	H	H	
20	Br	0	H	H	
21	H	1	H	H	
22	H	2	H	H	
23	H	0	Cl	CH <sub>3</sub>	
24	F	0	Cl	CH <sub>3</sub>	
25	Cl	0	Cl	CH <sub>3</sub>	
26	H	2	Cl	CH <sub>3</sub>	

Fig. 7 SARs of coumarin based compounds (13–26).

Despite having a similar overall folding structure, MAO-A and MAO-B share 70% sequence similarity. The availability of structural data has facilitated the development of isoform-selective MAO inhibitors through rational drug design.<sup>57</sup> The design strategy for MAO inhibitors requires a careful consideration of selectivity between MAO-A and MAO-B, reversibility, bioavailability, and safety to meet the therapeutic needs for conditions such as depression, Parkinson's disease, and other neuropsychiatric disorders. Recently, the design strategy for the treatment of neurological disease focused on the synthesis of compounds with multitargeting such as MAO and CAs, and MAO and AChE.<sup>58</sup>

Cholinesterases (ChEs) are essential enzymes involved in several critical fields, including neurobiology, toxicology, and pharmacology. Among these, acetylcholinesterase (AChE) and butyrylcholinesterase (BChE) are two key groups that play significant roles in the functioning and health of humans and animals.<sup>59</sup> AChE, also referred to as true cholinesterase, is predominantly found in the CNS.<sup>60</sup> AChE is attached to the cell membranes of excitable tissues and plays a key role in nerve signal transmission. Its primary biological function is

to catalyze the breakdown of the neurotransmitter acetylcholine into choline, a process essential for a cholinergic neuron to return to its resting state after being activated. AChE is also present in the membranes of red blood cells, where it is referred to as erythrocyte ChE. BChE, also known as pseudocholinesterase, plasma, or serum ChE, is mainly found in plasma, liver, and muscle tissues. Its exact biological function, however, remains unclear. Although BChE has a molecular structure similar to AChE, it differs in its substrate specificities. AChE primarily hydrolyzes acetyl esters, such as acetylcholine, whereas BChE predominantly hydrolyzes butyrylcholine, although there is some overlap in their substrate preferences.<sup>61</sup> The design strategy of ChE inhibitors, which target both AChE and BChE, is crucial for developing therapies for neurodegenerative diseases (like Alzheimer's disease), antidotes for neurotoxins, and insecticides. The design of these inhibitors involves several key aspects, focusing on maximizing potency, selectivity, and bioavailability and minimizing side effects. In recent decades, the primary approach for drug discovery has shifted to designing highly selective drug molecules that target a

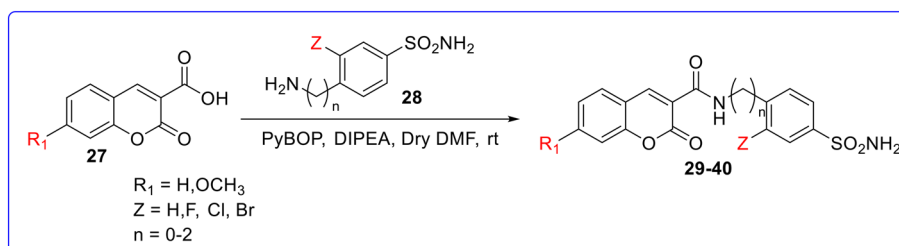


Fig. 8 Synthesis of compounds 29–40.



single drug target.<sup>62</sup> However, in many cases, the efficacy of single-target drugs often fails to meet people's expectations. Due to the diversity of the pathogenesis of neurodegenerative diseases, the molecules that regulate the activity of single-target proteins may not significantly change the progression of the disease.<sup>63</sup> To improve efficacy, many may consider combining drugs. However, drug combinations can increase the risk of adverse reactions due to contraindications and potential drug-drug interactions.<sup>64</sup> In 2005, Morphy *et al.* introduced a multi-target drug therapy strategy (MTDTS), offering a novel approach to drug discovery.<sup>65</sup> As a result, the creation of synergistic multi-target inhibitors has emerged as a more promising strategy for treating diseases, particularly those caused by complex factors like AD.<sup>66</sup> AChE is regarded as a primary target, and it can be combined with other targets to design and synthesize multi-target drug ligands (MTDLs), such as AChE with CAs, AChE with BACE-1, AChE with MAO, and AChE with PDE. Therefore, we reviewed studies from the past decade, summarizing the design concepts and structure-activity relationship (SAR) that may offer new pathways for the future development of small molecule candidate drugs used in the treatment of neurodegenerative disease. To the best of our knowledge, this is the first review which covers the chemistry and SAR of dual acting carbonic anhydrase inhibitors with MAO and ChE.

## 2. Dual acting carbonic anhydrase inhibitors

### 2.1. Dual acting carbonic anhydrase with monoamine oxidase inhibitors

Giovannuzzi *et al.* (2024) designed and synthesized various dual acting CAs-MAO-B inhibitors and evaluated their inhibitory activity against an SH-SY5Y human neuroblastoma cell model exposed to toxic A $\beta$  peptides *in vitro*.<sup>67</sup> All the design compounds were synthesized by a linking strategy, where two distinct scaffolds, known for their MAO-B and CAs inhibition, were connected by a linker. They conjugate benzopyrone scaffolds (chalcone or coumarin) as MAO-B inhibitors with a benzenesulfonamide motif (CAs inhibitor) at different positions, using a linker for the connection (Fig. 5).

By using this design strategy, they synthesized different sets of coumarin-benzenesulphonamide and chromone-benzenesulphonamide derivatives. The first set of derivatives was synthesized by reacting 7-hydroxycoumarin with benzenesulfonamide bearing a 4-(2-chloroacetamide) moiety in the presence of K<sub>2</sub>CO<sub>3</sub> as a base in anhydrous DMF at 40 °C to obtain hybrid compounds 13–26 (Fig. 6). Among the synthesized derivatives, compound 13 was found to be most potent molecule with a  $K_i$  value ranging from 0.8 to 9.4 nM against CA II, VA and VII as compared to standard drugs acetazolamide (AAZ) with a  $K_i$  value = 2.5 to 63 nM and methazolamide (MTZ) with a  $K_i$  value = 2.1 to 65 nM. Compound 14, featuring a 3-fluoro-sulfanilamide scaffold connected to an unsubstituted coumarin fragment, demonstrated good inhibitory activity against CAs II, VA, VB,

Com	Z	n	R <sub>1</sub>	
29	F	0	H	Most potent CAs inhibitor $K_i$ value = 0.4 to 11 nM (CAII, VA, VII, XII)
30	H	2	H	$K_i$ value = 2.4 nM (CA-II), 9.3 nM (CA-XII)
			AAZ	$K_i$ = 2.5 to 63 nM
			MTZ	$K_i$ = 2.1 to 65 nM
31	H	0	H	
32	Cl	0	H	
33	Br	0	H	
34	H	1	H	CAs inhibitory activity decreases
35	H	0	H	
36	F	0	OCH <sub>3</sub>	Most potent MAO-B inhibitor IC <sub>50</sub> = 14.9 nM
37	Cl	0	OCH <sub>3</sub>	
38	Br	0	OCH <sub>3</sub>	
39	H	1	OCH <sub>3</sub>	
40	H	2	OCH <sub>3</sub>	Most active compound against CA-XII $K_i$ value = 7.0 nM

Fig. 9 SARs of compounds 29–40.

and VII, with a  $K_i$  value ranging from 8.9 to 25.5 nM. The substitution of the fluorine atom with hydrogen or other halogen (compounds 18–20) reduces the CA inhibitory activity. A similar decrease in activity was observed with the elongation of the spacer between the amide linker and the CAI portion (compounds 21 and 22), or with the substitution of the coumarin scaffold with a 3-chloro-4-methyl pattern (compounds 23–26). All the synthesized compounds showed very less or no MAO inhibitory activity as compared to standard drugs clorgyline (CLO) with an IC<sub>50</sub> value of 15 610 nM for MAO-A and 47.6 nM for MAO-B and selegiline (SEL) with an IC<sub>50</sub> value of 3.0 nM for MAO-A and 2501 nM for MAO-B (Fig. 7).

The second set of derivatives was synthesized by a coupling reaction between 3-carboxycoumarin and amine-bearing benzenesulfonamide in the presence of PyBOP as a coupling reagent and DIPEA as a base, in anhydrous DMF to give compounds 29–40 (Fig. 8). Compound 29 with a 3-fluoro-sulfanilamide scaffold connected to an unsubstituted coumarin fragment was the most effective inhibitor of CA II ( $K_i$  value = 0.4 nM), CA-VA ( $K_i$  value = 6.9 nM), and CA-VII ( $K_i$  value = 11 nM) among the produced derivatives. The elongation of the spacer (ethylene group) between the amide linker and CAI portion (30) increases the CA inhibitory activity. The substitution of the fluorine atom with hydrogen or other halogen atom decreases the CA inhibitory activity with respect to standard drugs AAZ ( $K_i$  value = 2.5 to 63 nM) and MTZ ( $K_i$  value = 2.1 to 65 nM). Similarly, the elongation

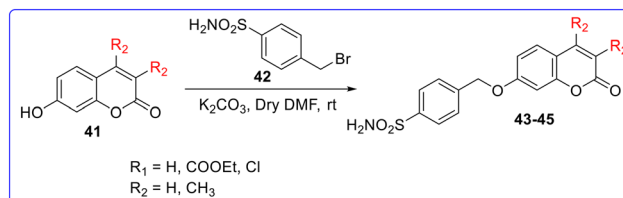


Fig. 10 Synthesis of compounds 43–45.

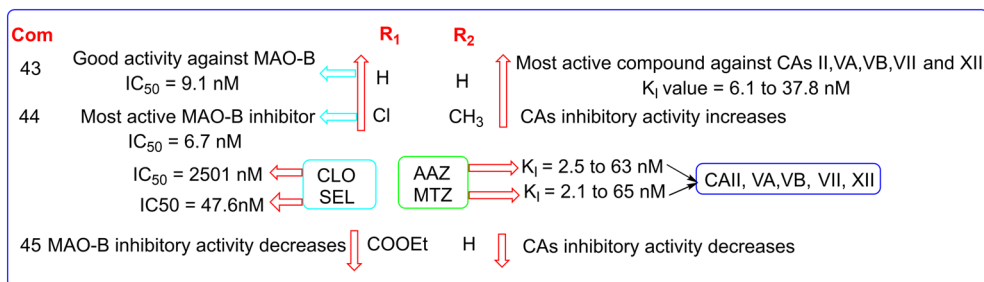


Fig. 11 SARs of coumarin based compounds (43–45).

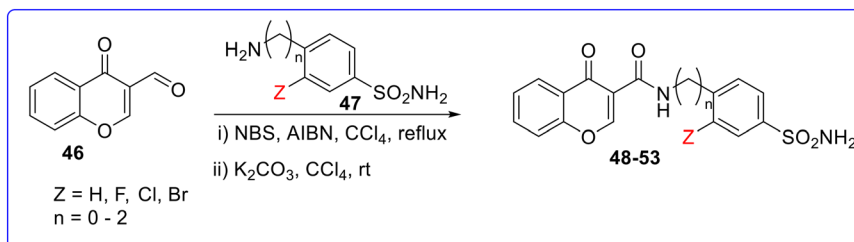


Fig. 12 Synthesis of compounds 48–53.

of the spacer between the amide linker and CAI portion (34) or substitution at the coumarin scaffold with a 7-OCH<sub>3</sub> group (35–40) dramatically decreases the CA inhibitory activity. Compound 40 ( $K_i$  value 7.0 nM) was found as the most active compound against CA-XII among the synthesized drugs but less than standard drugs AAZ ( $K_i$  value = 5.7 nM) and MTZ ( $K_i$  value = 3.4 nM). Some of the synthesized compounds showed increased MAO-B inhibitory activity as compared to the first set of derivatives. Among them, compound 36 was found as the most active compound against MAO-B with an IC<sub>50</sub> value of 14.9 nM (Fig. 9).

The third set of derivatives (43–45) was synthesized by reacting 7-hydroxycoumarin with 4-sulfamoylbenzyl bromide in the presence of K<sub>2</sub>CO<sub>3</sub> in dry DMF (Fig. 10). Among the synthesized derivatives, compound 43 was found as the most potent CAI against CA-II, VA, VB, VII and XII with  $K_i$  values of 6.1, 37.1, 15.5, 8.2 and 37.8 nM, respectively. Substitution of chlorine at R<sub>1</sub> and the methyl group at the R<sub>2</sub> position (compound 46) showed good inhibitory activity against CAs with a  $K_i$  value ranging from 5.6 to 66.1 nM. Substitution of the COOEt group at R<sub>1</sub> and hydrogen at the R<sub>2</sub> position decreases the CA inhibitory activity with respect to standard drugs AAZ ( $K_i$  value = 2.5 to 63 nM) and MTZ ( $K_i$  value = 2.1 to 65 nM). Notably, compounds 43 and 44 exhibited highly potent MAO-B inhibition, with IC<sub>50</sub> values of 9.1 and 6.7 nM, respectively (Fig. 11).

The fourth set of derivatives (48–53) were synthesized by converting the aldehyde group of compound 46 (chromone derivatives) into acyl bromide through a free radical reaction involving NBS and AIBN in CCl<sub>4</sub>, followed by a coupling reaction with benzenesulfonamide in the presence of K<sub>2</sub>CO<sub>3</sub> as a base in CCl<sub>4</sub> (Fig. 12). All the synthesized chromone

derivatives showed less CA inhibition as compared to coumarin derivatives (second set). Among the synthesized derivatives, compound 48 was found as the most potent CAI with a  $K_i$  value ranging from 8.3 to 58.4 nM. The elongation of the spacer between the amide linker and CAI portion was responsible for increasing CA inhibitory activity. The fluorine substituted compound 50 showed good inhibitory activity with a  $K_i$  value of 6.4 nM. The substitution of fluorine with hydrogen or other halogen atom dramatically decreases the CA inhibitory activity. The unsubstituted compound 49 showed good MAO-B inhibitory activity with an IC<sub>50</sub> value of 32.6 nM (Fig. 13).

Carradori *et al.* (2022) synthesized various resveratrol (RSV) analogues (Fig. 14) as dual inhibitors of MAO-B and CAs and evaluated their inhibitory activity by a stopped-flow technique or the esterase activity assay.<sup>68–70</sup> All the derivatives were synthesized by a previously reported method.<sup>71–74</sup> Among the synthesized derivatives, compound 55 was found as the most potent molecule with IC<sub>50</sub> values of 0.433 μM (MAO-A) and 0.01

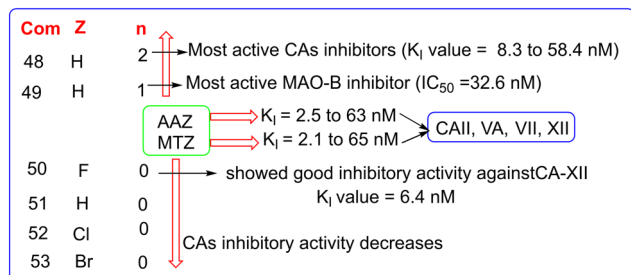


Fig. 13 SARs of chromone based compounds 48–53.

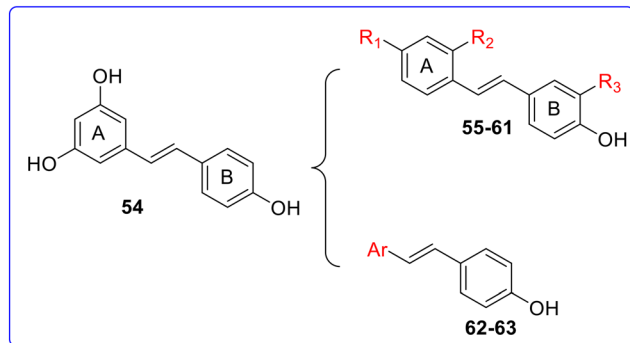


Fig. 14 Structure and synthesized derivatives of RSV.

$\mu\text{M}$  (MAO-B) with respect to the parent compound RSV with  $\text{IC}_{50}$  values of  $13.5 \mu\text{M}$  (MAO-A) and  $>100 \mu\text{M}$  (MAO-B) and standard drug isatin with  $\text{IC}_{50}$  values of  $8.43 \mu\text{M}$  (MAO-A) and  $3.90 \mu\text{M}$  (MAO-B) (Fig. 15). Substitution of the  $\text{CF}_3$  group at  $\text{R}_1$  and the chlorine atom at the  $\text{R}_3$  position is responsible for the inhibitory activity of compound 55. It also showed good inhibitory activity against CAs with  $\text{IC}_{50}$  values of  $15.6 \mu\text{M}$  (CA II),  $70.9 \mu\text{M}$  (CA VA),  $36.2 \mu\text{M}$  (CA VB),  $0.7 \mu\text{M}$  (CA VII), and  $6.9$

$\mu\text{M}$  (CA XII) but less than those of parent molecule RSV and standard drug AAZ with  $\text{IC}_{50}$  values ranging from  $0.9$  to  $2.8 \mu\text{M}$  and  $0.006$  to  $0.054 \mu\text{M}$ , respectively. The substitution of  $\text{CF}_3$  with other electron-withdrawing groups (EWGs) like  $-\text{CN}$  or  $-\text{Cl}$  at the  $\text{R}_1$  position, while keeping a halogen ( $-\text{Cl}$ ) or hydrogen at the  $\text{R}_2$  or  $\text{R}_3$  positions (compounds **56–58**), demonstrated good inhibitory activity against MAO, but resulted in a decrease in CA inhibitory activity. The substitution of  $\text{CF}_3$  with hydrogen at the  $\text{R}_1$  position (**61**) retained the MAO-A and MAO-B inhibitory activity, whereas substituting  $-\text{Cl}$  with hydrogen at the  $\text{R}_3$  position (compound **62**) reduced the MAO-B inhibitory activity compared to the standard drug isatin. Similarly, substitution of the naphthyl group at the Ar position (**60**) retained the MAO-B inhibitory activity while the substitution of the pyridyl group at the Ar position (**63**) decreases the MAO-B inhibitory activity. Substitution of electron withdrawing  $\text{CF}_3$  with an electron donating group (EDG) such as  $-\text{OCH}_3$  at the  $\text{R}_1$  position and hydrogen at  $\text{R}_2$  and  $\text{R}_3$  positions (**59**) retained the MAO-B inhibitory activity. All the synthesized RSV derivatives showed less CA inhibitory activity with respect to parent molecule RSV and standard drug AAZ. The molecular docking study of compound 55 for MAO-A and MAO-B was conducted using

Com	$\text{R}_1$	$\text{R}_2$	$\text{R}_3$	Ar	
55	$\text{CF}_3$	H	Cl	-	Most potent molecule $\text{IC}_{50} = 0.433 \mu\text{M}$ (MAO-A), $0.01 \mu\text{M}$ (MAO-B) $\text{IC}_{50} = 6.9-70.9 \mu\text{M}$ (CA II, VA, VB, VII, XII)
56	Cl	Cl	H	-	
57	CN	H	H	-	
58	Cl	Cl	Cl	-	MAO inhibitory activity increases
59	$\text{OCH}_3$	H	H	-	
60	-	-	-	Naphthyl	
61	H	H	Cl	-	
62	$\text{CF}_3$	H	H	-	Isatin $\text{IC}_{50} = 8.43 \mu\text{M}$ (MAO-A), $3.90 \mu\text{M}$ (MAO-B)
63	-	-	-	Pyridyl	RSV $\text{IC}_{50} = 13.5 \mu\text{M}$ (MAO-A), $>100 \mu\text{M}$ (MAO-B) MAO inhibitory activity decreases

Fig. 15 SARs of RSV derivatives.

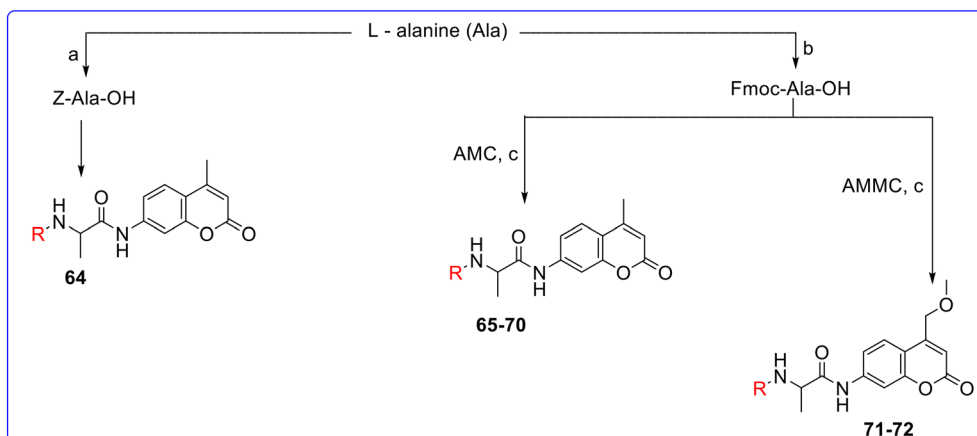
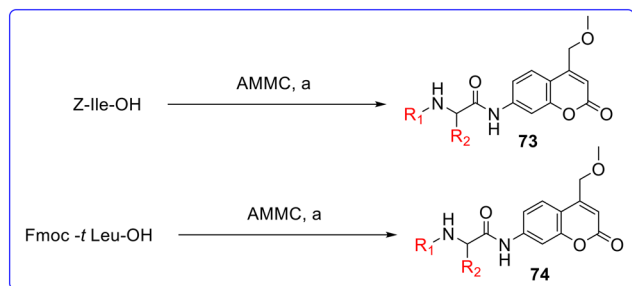


Fig. 16 Synthesis of coumarin derivatives (**64–72**); reagents and conditions: (a)  $\text{Z-Cl}$ ,  $1 \text{ N NaOH}$ ,  $0^\circ\text{C}$ ,  $2 \text{ h}$ , then  $\text{r.t.}$ ,  $16 \text{ h}$ ; (b)  $\text{Fmoc-OSu}$ ,  $\text{TEA}$ ,  $\text{H}_2\text{O}/\text{THF}$  ( $2:1$ ),  $\text{r.t.}$ ,  $4 \text{ h}$ ; (c)  $\text{IBCF}$ ,  $\text{TEA}$ , dry  $\text{THF}$ ,  $-10^\circ\text{C}$  under  $\text{N}_2$ ,  $1 \text{ h}$ , then  $\text{r.t.}$ ,  $24 \text{ h}$ .





**Fig. 17** Synthesis of coumarin derivatives (**73** and **74**). Reagents and conditions: (a) IBCF, TEA, dry THF,  $-10\text{ }^{\circ}\text{C}$  under  $\text{N}_2$ , 1 h, then r.t., 20 h.

Schrödinger Life-Sciences Suite 2021-4 (Maestro v13), with PDB codes of 2Z5X and 2V5Z, respectively. Interestingly, the docking score of compound **55** was found to be similar to the standard drug safinamide (10.336 for MAO-A, 10.375 for MAO-B). The docking study of compound **55** for CAs was performed in GOLD 5.1 program, using the PLP scoring function. The crystal structures of CA I (PDB code 1AZM), CA II (PDB code 4E3H), CA VII (PDB code 3MDZ), CA IX (PDB code 5FL4), and CA XII (PDB code 1JCZ) were obtained from the Protein Data Bank, while previously developed homology models were used for CA VA and CA VB.<sup>75,76</sup> The docking study of compound **55** revealed

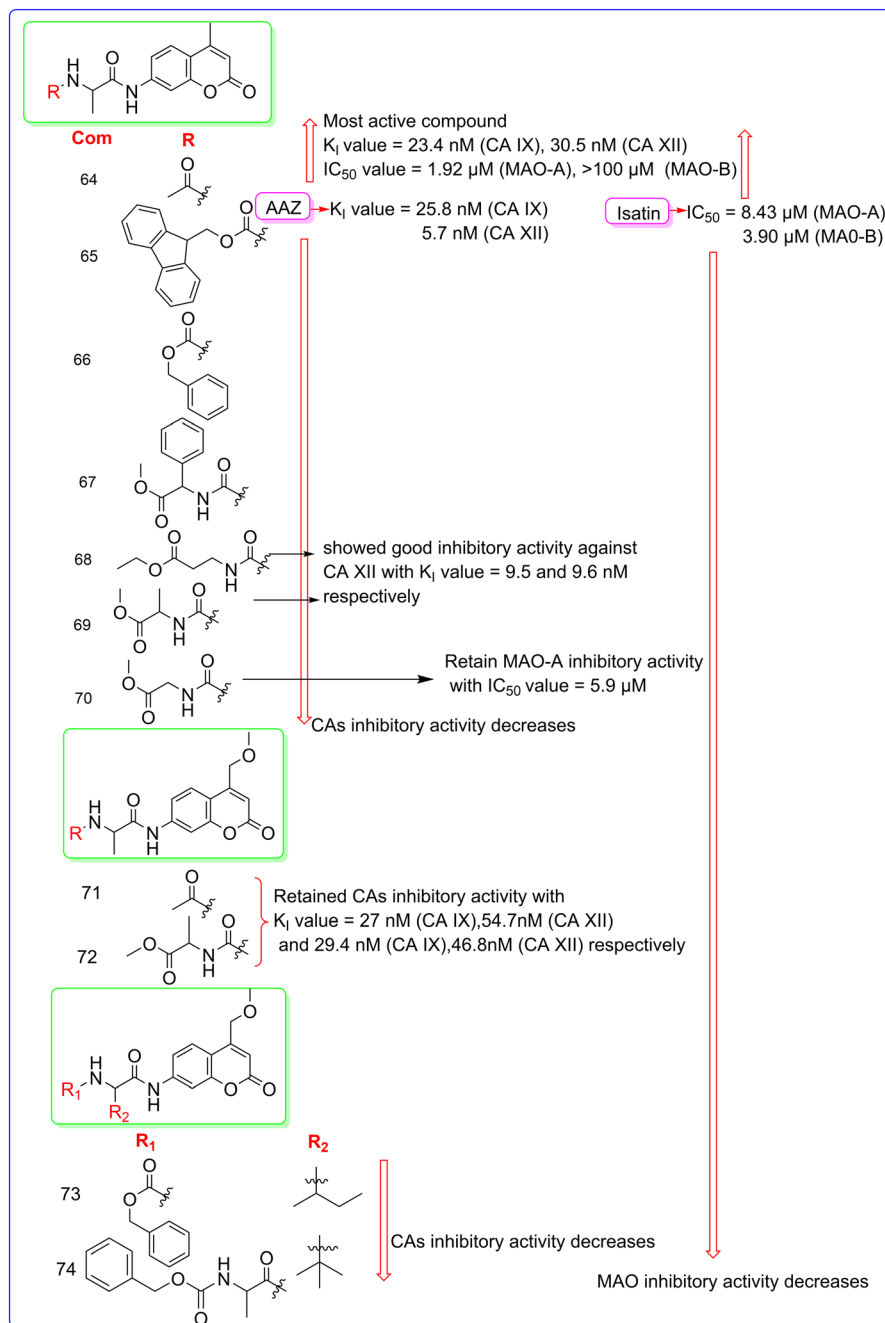


**Fig. 18** SARs of coumarin derivatives.

demonstrated good MAO inhibition activity with  $IC_{50}$  values of 1.92  $\mu M$  (MAO-A) and  $>100 \mu M$  (MAO-B) with respect to standard drug isatin having  $IC_{50}$  values of 8.43  $\mu M$  (MAO-A) and 3.90  $\mu M$  for MAO-B. The substitution of methyl ketone at position R is responsible for the good inhibitory activity of compound **64**. Substitution of methyl ketone with other groups (**65–70**) dramatically decreased the potency of the molecule except compounds **68** and **69** which showed good inhibitory activity against CA XII with  $K_I$  values of 9.5 and 9.6 nM, respectively. Substitution of methyl ketone and methyl acetylalaninate at position R of AMMC derivatives (**71** and **72**) retained the CA inhibitory activity. Further substitution of butane and isobutane at the  $R_2$  position decreased the CA inhibitory activity. Substitution of methyl ketone with other groups (**65–74**) decreased the MAO-A and MAO-B inhibitory activity (Fig. 18). The molecular docking study was performed on Schrödinger Life-Sciences Suite 2021-4 (ref. 79) by using PDB ID 2Z5X (MAO-A), 2V5Z (MAO-B), 6F3B (CA I), 5BNL (CA II), 6G9U (CA IX) and 5LL5 (CA XII).

## 2.2. Dual acting carbonic anhydrase with cholinesterase (ChE) inhibitors

Several pyrazole carbamide derivatives are designed and synthesized as selective inhibitors of carbonic anhydrase and cholinesterase (Durgun *et al.*, 2024), and their inhibitory action against acetylcholinesterase (AChE), butyrylcholinesterase (BChE), CA I, and CA II is assessed *in vitro*.<sup>80</sup> All the pyrazole carboxamide derivatives were synthesized by the reaction of diazotization of appropriate sulphonamide derivative **75** to give diazonium salt **76**, followed by the reaction with malononitrile in sodium acetate in methanol at 0–10 °C to give **77**. On reacting compound **77** with compound **78** in alcohol at 60 °C,

**Fig. 19** Synthesis of pyrazole carboxamide derivatives.

pyrazole carboxamide derivatives (**79–90**) were obtained in desirable yields of 62–85% (Fig. 19). All the synthesized compounds showed good inhibitory activity against ChEs having  $K_i$  values ranging from 6.60–14.15 nM (AChE) and 54.87–137.20 nM (BChE) and CAs having  $K_i$  values ranging from 10.69–70.87 nM (CA I) and 20.01–56.6 nM (CA II) as compared to standard drugs tacrine ( $K_i$  value = 112 nM for AChE, 172 nM for BChE) and AAZ ( $K_i$  value = 412 nM for CA I, 98.2 nM for CA II). Among the synthesized derivatives, compound **79** was found as the most potent molecule against ChEs with  $K_i$  values of 6.60 nM for AChE and 68.9 nM for BChE. The substitution of

4,6-dimethylpyrimidin-2-amine at the  $R_1$  position and 1,2-dichlorobenzene at the  $R_2$  position is responsible for the most potent inhibitory activity of compound **79** against ChEs. Compound **87** was found as the most active compound against CAs with  $K_i$  values of 10.6 nM (CA I) and 20.01 nM (CA II) as compared standard drug AAZ having  $K_i$  values of 412 nM for CA I and 98.2 nM for CA II. The substitution of guanidine at the  $R_1$  position and *p*-methyl benzene at the  $R_2$  position is responsible for the good inhibitory activity against CAs (Fig. 20). The docking study of the most active compounds (**79**, **83**, **84** and **80**) was performed by using Small-Molecule Drug Discovery Suite

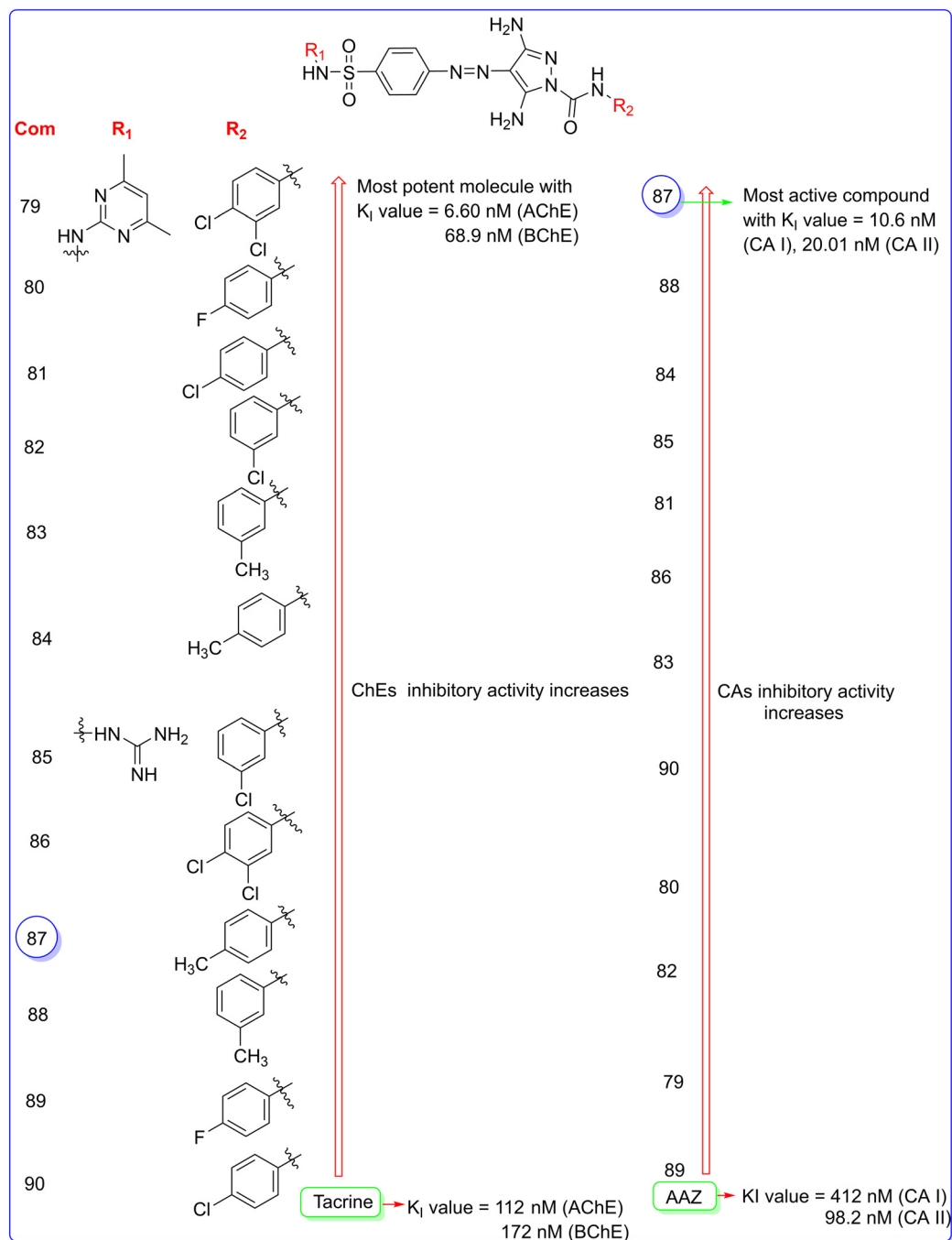


Fig. 20 SARs of pyrazole carboxamide derivatives.

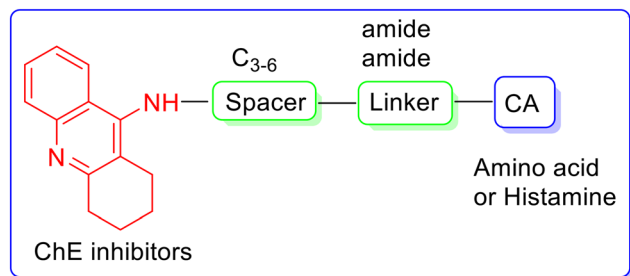


Fig. 21 Drug design strategy of dual acting CA activators and AChE inhibitors.

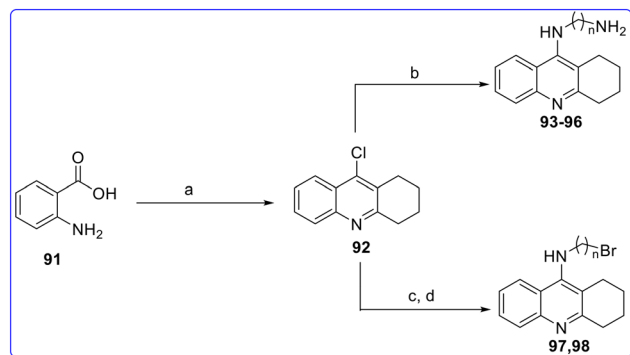


Fig. 22 Synthesis of intermediate compounds (91–98). Reagents and conditions: (a) cyclohexanone,  $\text{POCl}_3$ , 0 to 115 °C, (b) 1- $\omega$ -diaminoalkane, KI, phenol, 180 °C, (c)  $\omega$ -aminoalkanol-1-ol, KI, phenol, 180 °C, and (d)  $\text{CBr}_4$ ,  $\text{PPh}_3$ , DMF, rt.

2023-2 with PDB ID 7XN1 (AChE) and 4BDS (BChE), and 1AZM (CA I) and 3HS4 (CA II). The docking methodology's reliability was confirmed by the low RMSD values (0.26, 0.12, 0.22, and 0.99 Å for 7XN1, 4BDS, 1AZM, and 3HS4, respectively) and the ability of the docking poses of the co-crystallized ligands to accurately replicate all key interactions. Compounds **79**, **83**, **84** and **80** formed primary interactions *via* hydrogen bonding and pi-pi stacking. These inhibitors exhibited docking scores of  $-9.686$ ,  $-5.306$ ,  $-2.958$ , and  $-6.376$  kcal mol $^{-1}$  with 7XN1, 4BDS, 1AZM, and 3HS4, respectively. The result of *in silico* and *in vitro* study supported to each other (Fig. 21).

Nocentini *et al.* (2024) designed and synthesized various dual acting CA activators and AChE inhibitors, and evaluated their biological activity *in vitro*.<sup>81</sup> The intermediate 9-chloro-

1,2,3,4-tetrahydroacridine (**92**) was synthesized through the condensation of anthranilic acid (**91**) with cyclohexanone in the presence of  $\text{POCl}_3$  at 115 °C. Subsequently, intermediate **92** was reacted with the appropriate 1, $\omega$ -diaminoalkane in the presence of potassium iodide in phenol at 180 °C, yielding the aminoalkyl TAC intermediates **93–96** (Fig. 22). The  $\omega$ -bromoalkyl intermediates **97** and **98** were prepared *via* two-step synthesis. First, intermediate **92** was reacted with the appropriate amino alcohol in the presence of KI in phenol at 180 °C. This was followed by the Appel reaction using  $\text{CBr}_4$  and  $\text{PPh}_3$  in DMF at room temperature (Fig. 22). Intermediates **93–96** were coupled with commercially available protected L-amino acids using PYBOP as the coupling agent and DIPEA in DMF, resulting in the formation of amide compounds **99–123**. Specifically, compounds **99–112** and **121–123** were synthesized using *N,N'*-diBoc-L-histidine and *N*-Boc-*N'*-Cbz-L-lysine, respectively, to prevent undesired side reactions. The *N*-Boc groups of compounds **99–123** were subsequently removed by treatment with 1.25 M methanolic HCl at room temperature, yielding the corresponding amine compounds **124–138** (Fig. 23). Intermediates **97** and **98** underwent an  $\text{S}_{\text{N}}2$  reaction with methyl ester L-amino acids in the presence of  $\text{K}_2\text{CO}_3$  and KI, resulting in the formation of amine-linked hybrids **139–146** (Fig. 24). Similarly, the TAC hybrids **147** and **148** were synthesized using histamine dihydrochloride (Fig. 25). Finally, the tyrosine derivatives **149** and **150** were synthesized by reacting intermediates **97** and **98** with *N*-Boc-L-tyrosine methyl ester. The *N*-Boc groups of compounds **149** and **150** were subsequently removed by treatment with 1.25 M HCl in methanol at room temperature, yielding hybrids **151** and **152**. All the synthesized compounds showed less CA activator activity against CA I and CA II as compared to standard drug L-phenylalanine having  $K_{\text{A}}$  values of 70 nM and 13 nM, respectively. Among the synthesized derivatives, compound **148** was found as the most active compound against CA I with a  $K_{\text{A}}$  value of 236 nM but less than standard drug L-phenylalanine. Similarly, compound **126** was found as the most active compound against CA II having a  $K_{\text{A}}$  value of 65.1 nM but less than standard drug L-phenylalanine. Among the synthesised derivatives, compounds **135** and **124** were found as the most potent CA activators against CA IV with  $K_{\text{A}}$  values of 541 nM and 619 nM, respectively, as compared to standard drug L-Phe having a  $K_{\text{A}}$  value of 36 000 nM. Similarly, compounds **135** and **127** were found as the most potent CA activators against CA VB with  $K_{\text{A}}$  values of 353 nM and 544 nM, respectively, as

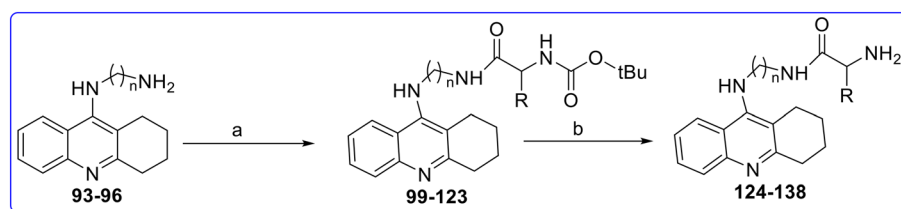
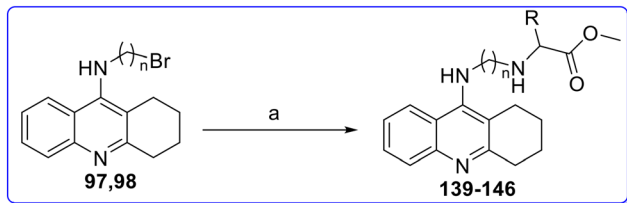
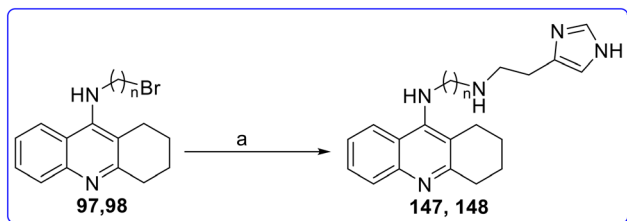


Fig. 23 Synthesis of dual acting CA activators and AChE inhibitors (**124–138**). Reagents and conditions: (a) protected L-amino acid (*N,N'*-diBoc-L-histidine, *N*-Boc-L-phenylalanine, *N*-Boc-L-tryptophan, *N*-Boc-*N'*-Cbz-L-lysine), PYBOP, DIPEA, DMF, rt and (b) 1.25 M methanolic HCl, 0 °C to rt.



**Fig. 24** Synthesis of dual acting CA activators and AChE inhibitors (**139–146**). Reagents and conditions: (a) L-amino acid methyl ester (L-histidine, L-phenylalanine, L-tryptophan, and *N'*-Cbz-L-lysine),  $K_2CO_3$ , KI, DMF, rt.



**Fig. 25** Synthesis of dual acting CA activators and AChE inhibitors (**147** and **148**). Reagents and conditions: (a) histamine dihydrochloride,  $K_2CO_3$ , KI, DMF, rt.

compared to standard drug L-phenylalanine having a  $K_A$  value of 10 000 nM. Among the synthesized derivatives, compounds **127** and **126** were found as the most potent CA activators against CA VII with  $K_A$  values of 82.8 nM and 96.4 nM, respectively, as compared to standard drug L-phenylalanine having a  $K_A$  value of 10 000 nM. All derivatives, except for the histamine-derived compound **148**, demonstrate selective inhibition of BChE over AChE, resembling the lead compound tacrine. Among the synthesized compounds, compounds **148** and **135** showed the most potent inhibitory activity against AChE with  $IC_{50}$  values of 2.2  $\mu$ M and 2.4  $\mu$ M, respectively, as compared to standard drug tacrine having an  $IC_{50}$  value of 33.9  $\mu$ M. Similarly, compounds **151** and **100** showed the most potent inhibitory activity against BChE with  $IC_{50}$  values of 0.048  $\mu$ M and 0.064  $\mu$ M, respectively, as compared to standard drug tacrine having an  $IC_{50}$  value of 3.9  $\mu$ M (Fig. 27). Docking study was performed in the Maestro Schrödinger suite against hCA II (PDB: 2ABE),<sup>82</sup> hCA VII (PDB: 6H38),<sup>83</sup> hAChE (PDB: 4BDT)<sup>84</sup> and hBChE (PDB: 6IOB) (Fig. 26).<sup>85</sup>

Berrino *et al.* (2023) designed and synthesized various alkyl substituted coumarins and evaluated their biological activity *in vitro* against CAs, MAO-A, MAO-B, AChE and BChE.<sup>86</sup> The target compounds **154** and **155** were synthesized by reacting starting material **153** with 5-chloropent-1-yne and 6-chlorohex-1-yne, respectively. The compound **156** was reacted with 3-bromoprop-1-yne and 1-bromobut-2-yne in dry DMF at 150 °C to give compounds **157** and **158**, respectively. Compounds **160–164** were obtained by a similar reaction between compound **159** and 3-bromoprop-1-yne, 1-bromobut-2-yne, 1-bromopent-2-yne, 5-chloropent-1-yne, and 6-chlorohex-1-yne in dry DMF at 150 °C (Fig. 28). All the synthesized derivatives showed less CA I, CA II, CA VII inhibitory activity as compared to standard drug AZZ having  $K_I$  values of 250 nM, 12.1 nM, and 2.5 nM, respectively. Among the synthesized derivatives, compound **154** was found as the most active CA I inhibitor with a  $K_I$  value of 6262 nM, but less active than standard drug AZZ. All the synthesized compounds showed less CA II inhibitory activity with  $K_I$  values of >10 000 nM as compared to standard drug AZZ. Among the synthesized derivatives, compound **155** was found as the most active CA VII inhibitor with a  $K_I$  value of 46.93 nM, but less active than standard drug AZZ. Compound **155** also showed the most potent inhibitory activity against CA IX with a  $K_I$  value of 9 nM as compared to standard drug AZZ having a  $K_I$  value of 25.8 nM. The substitution of the hex-1-yne group at the  $R_1$  position is responsible for the most potent inhibitory activity of compound **155**. Among the synthesized derivatives, compound **158** showed the most potent inhibitory activity against CA XII with a  $K_I$  value of 4.3 nM as compared to standard drug AZZ having a  $K_I$  value of 5.7 nM. Substitution of the but-2-yne group at the  $R_1$  position is responsible for the most potent inhibitory activity of compound **158**. All the synthesized derivatives showed less AChE and BChE inhibitory activity as compared to standard drug galantamine having  $IC_{50}$  values of 1.29  $\mu$ M (AChE) and 5.4  $\mu$ M (BChE). All the synthesized compounds showed less AChE inhibitory activity with  $IC_{50}$  values of >100  $\mu$ M as compared to standard drug galantamine. Among the synthesized derivatives, compound **155** was found as the most active compound with an  $IC_{50}$  value of 21  $\mu$ M, but less active than the standard drug. Among the synthesized derivatives, compound **164** was found as the most potent inhibitor against MAO-A and MAO-B with  $IC_{50}$  values of 0.65  $\mu$ M and 0.007  $\mu$ M, respectively, as compared

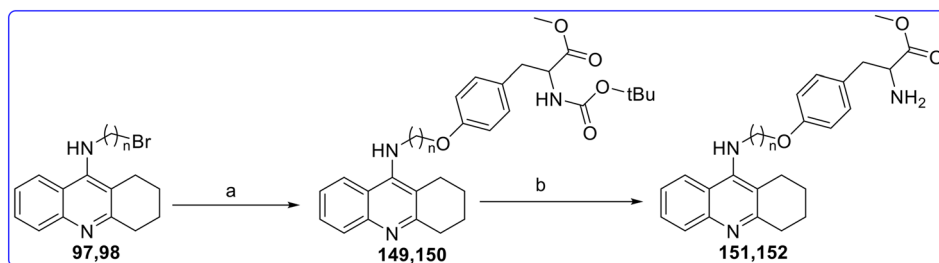


**Fig. 26** Synthesis of dual acting CA activators and AChE inhibitors (**149**, **152**). Reagents and conditions: (a) *N*-Boc-L-tyrosine methyl ester,  $K_2CO_3$ , KI, DMF, rt and (b) 1.25 M methanolic HCl, MeOH, 0 °C to rt.



Com	R	n	X
99		3	Boc
100		4	Boc
111		5	Boc
112		6	Boc
113		3	Boc
114		4	Boc
115		5	Boc
116		6	Boc
117		3	Boc
118		4	Boc
119		5	Boc
120		6	Boc
121		3	Boc
122		4	Boc
123		5	Boc
124		3	H
125		4	H
126		5	H
127		6	H

Com	R	n	X
128		3	H
129		4	H
130		5	H
131		6	H
132		3	H
133		4	H
134		5	H
135		6	H
136		3	H
137		4	H
138		5	H
139		5	-
140		6	-
141		5	-
142		6	-
143		5	-
144		6	-
145		5	-
146		6	-

Com	R	n	X
147	-	5	-
148	-	6	-
149	-	5	-
150	-	6	-
151	-	5	-
152	-	6	-

Fig. 27 SARs of dual acting CA activators and AChE inhibitors.

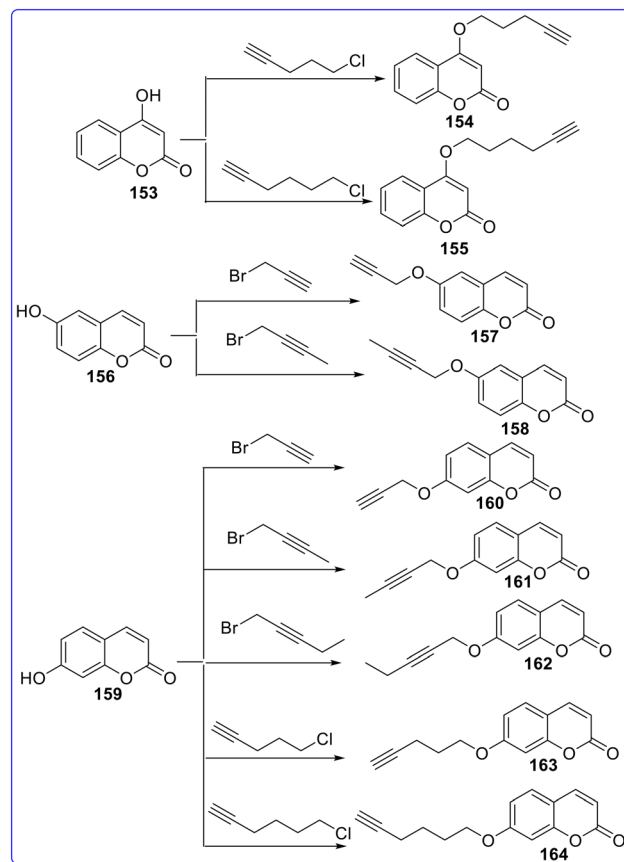


Fig. 28 Synthesis of alkyl substituted coumarins.

to standard drug curcumin having  $IC_{50}$  values of  $5.54 \mu M$  for MAO-A and  $4 \mu M$  for MAO-B. The substitution of the hex-1-ynyl group at the  $R_1$  position is responsible for the most potent inhibitory activity of compound **164** (Fig. 29).

Kurban *et al.* (2024) designed and synthesized a new class of sulfonamide derivatives and evaluated their inhibitory activity *in vitro* against CA I, CA II, AChE and BChE.<sup>87</sup> All the derivatives were synthesized by reacting compound **165** with phenolic aldehyde in TEA and DCM under reflux conditions to give compounds **166–170**, which were reacted with compound **171** in ethanol under reflux conditions to give target compounds **172–176**. Among the synthesized derivatives, compound **172** was found as the most potent CAI and CA II inhibitor with  $K_i$  values of  $8.98 nM$  and  $7.55 nM$ , respectively, as compared to standard drug AZZ having  $K_i$  values of  $250 nM$  for CA I and  $12 nM$  for CA II. Among the synthesized derivatives, compound **176** was found as the least active CAI and CA II inhibitor with  $K_i$  values of  $14.56 nM$  and  $13.85 nM$ , respectively. All the synthesized derivatives showed more AChE and BChE inhibitory activity as compared to standard drug neostigmine having  $K_i$  values of  $55.5 nM$  for AChE and  $33.3 nM$  for BChE. Among the synthesized derivatives, compound **174** was found as the most potent inhibitor against AChE and BChE with  $K_i$  values of  $12.90$  and  $6.21 nM$ , respectively, as compared to standard drug neostigmine. Among the synthesized derivatives, compound

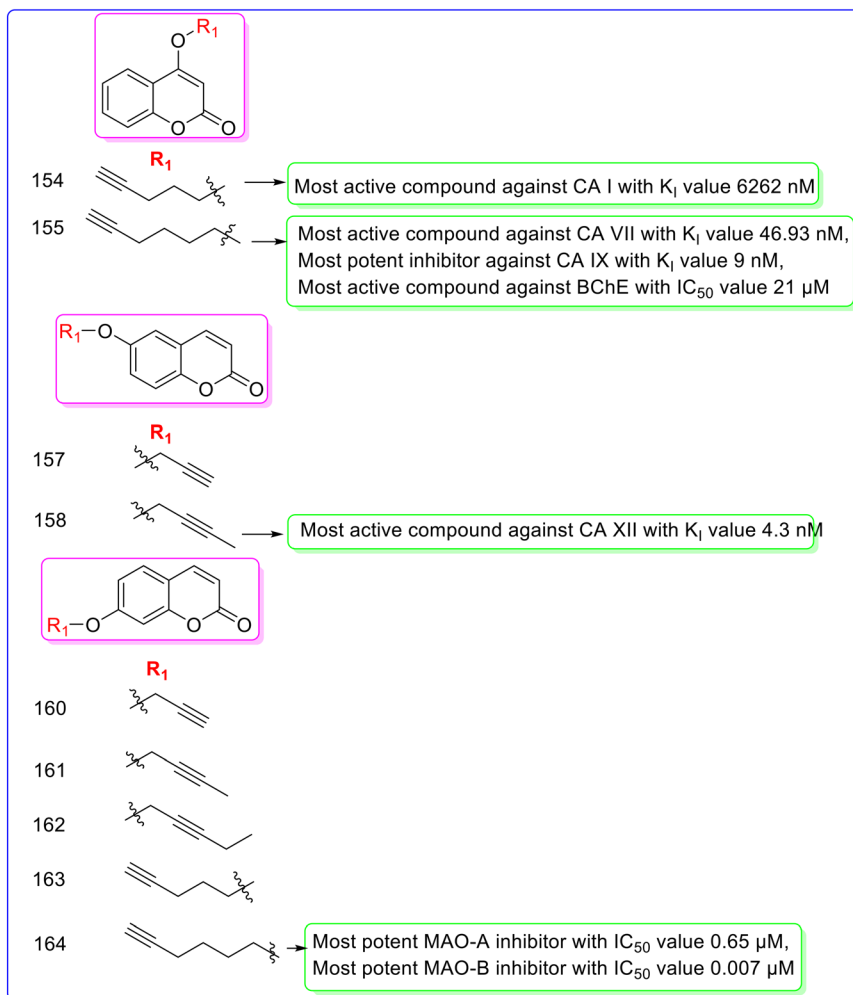


Fig. 29 SARs of alkyl substituted coumarins.

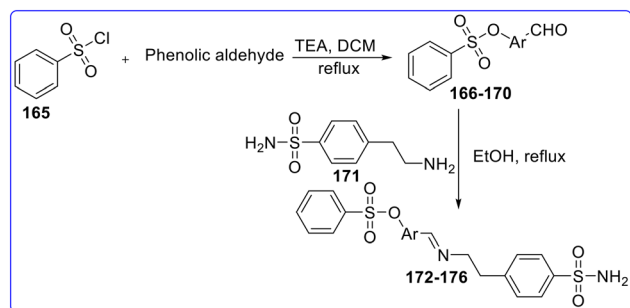


Fig. 30 Synthesis of a new class of sulfonamide derivatives.

172 showed the least potent inhibitory activity against AChE and BChE with  $K_i$  values of 16.38 and 14.52 nM, respectively. The docking study of the synthesized compound was performed by using PDB ID 1AZM for CA I, 4Q6E for CA II, 4EY7 for AChE and 4BDS for BChE. The docking scores of the most active compound 172 against CAs were found to be  $-5.209$  (CA I) and  $-5.863$  (CA II), and those of 174 against ChEs were found to be  $-10.500$  (AChE) and  $-6.825$  (BChE) (Fig. 30 and 31).

## Conclusion

Multi-target drug design (MTDD) offers a transformative approach to drug discovery, particularly for the treatment of complex and multifactorial diseases such as neurodegenerative disorders. By simultaneously modulating multiple biological targets, MTDD addresses the limitations of traditional single-target therapies, offering potential for improved therapeutic efficacy, reduced drug resistance, and more comprehensive disease management. In this article, we provided a summary of dual-acting drugs used in the treatment of neurodegenerative diseases over the past five years. In this article, we emphasize the design, synthesis, structure–activity relationships (SARs), docking study and biological activity of various dual-acting inhibitors targeting CAs, MAO, and ChE involved in the treatment of neurodegenerative diseases. The review also discusses key SAR studies that have guided the optimization of dual inhibitors, focusing on achieving selectivity and potency while minimizing off-target effects. SAR analysis of dual-acting drugs has proven essential in the development of effective therapeutic agents for neurodegenerative diseases. By understanding how structural modifications influence the biological activity and selectivity of dual inhibitors targeting

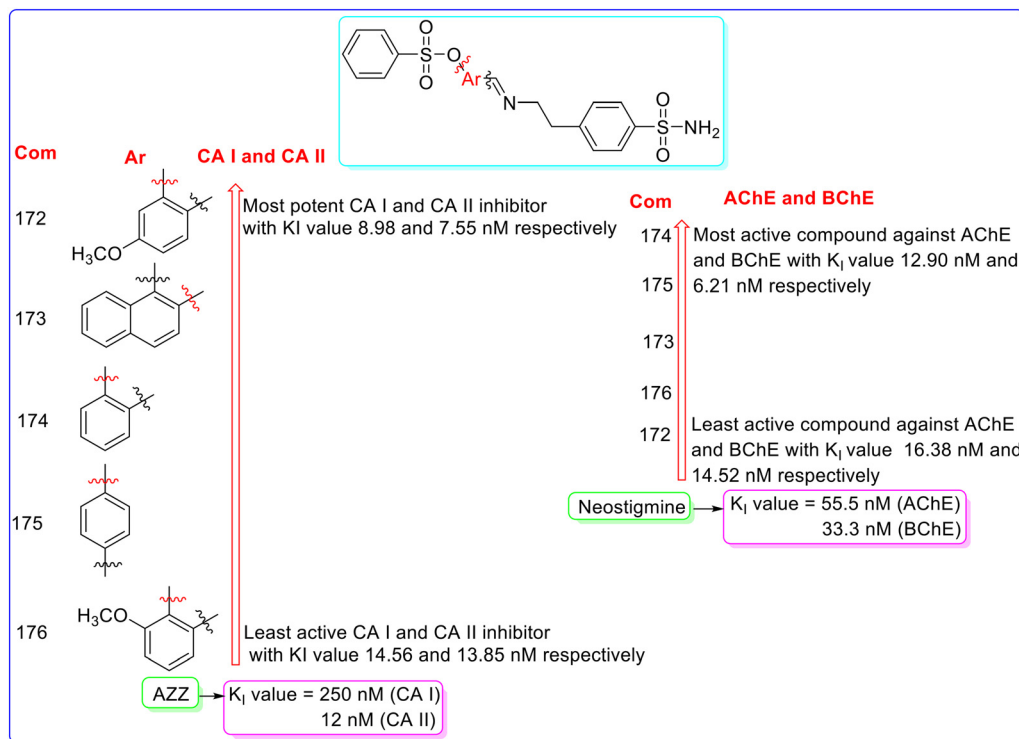


Fig. 31 SARs of a new class of sulfonamide derivatives.

multiple pathways, researchers can optimize drug candidates for enhanced efficacy and reduced side effects. The insights gained from SAR studies facilitate the fine-tuning of molecular properties, such as potency, selectivity, and pharmacokinetics, thereby addressing the complex nature of neurodegenerative conditions. As the landscape of drug discovery continues to evolve, integrating SAR findings with advanced computational methods and high-throughput screening will further enhance the design of dual-acting agents. While challenges such as maintaining selectivity for specific isoforms and managing potential off-target effects remain, ongoing research in SAR will be pivotal in overcoming these hurdles. Ultimately, the strategic application of SAR in the development of dual-acting drugs holds great promise for improving treatment outcomes for patients with neurodegenerative diseases, paving the way for more effective and personalized therapeutic strategies.

## Conflicts of interest

There is no conflict of interest to declare.

## Acknowledgements

This work was funded by the Deanship of Graduate Studies and Scientific Research at Jouf University under grant no. (DGSSR-2024-01-02246).

## References

- 1 H. Zheng, M. Fridkin and M. Youdim, *Pharmaceuticals*, 2014, **7**, 113–135.
- 2 E. Proschak, H. Stark and D. Merk, *J. Med. Chem.*, 2019, **62**, 420–444.
- 3 B. Mathew, D. G. T. Parambi, G. E. Mathew, Md. S. Uddin, S. T. Inasu, H. Kim, A. Marathakam, M. K. Unnikrishnan and S. Carradori, *Arch. Pharm.*, 2019, **352**(11), e1900177.
- 4 G. E. Konecny, M. D. Pegram, N. Venkatesan, R. Finn, G. Yang, M. Rahmeh, M. Untch, D. W. Rusnak, G. Spehar, R. J. Mullin, B. R. Keith, T. M. Gilmer, M. Berger, K. C. Podratz and D. J. Slamon, *Cancer Res.*, 2006, **66**, 1630–1639.
- 5 K. Li, L. A. Schurig-Briccio, X. Feng, A. Upadhyay, V. Pujari, B. Lechartier, F. L. Fontes, H. Yang, G. Rao, W. Zhu, A. Gulati, J. H. No, G. Cintra, S. Bogue, Y.-L. Liu, K. Molohon, P. Orlean, D. A. Mitchell, L. Freitas-Junior, F. Ren, H. Sun, T. Jiang, Y. Li, R.-T. Guo, S. T. Cole, R. B. Gennis, D. C. Crick and E. Oldfield, *J. Med. Chem.*, 2014, **57**, 3126–3139.
- 6 O. Benek, J. Korabecny and O. Soukup, *Trends Pharmacol. Sci.*, 2020, **41**, 434–445.
- 7 W. Löscher, *Front. Pharmacol.*, 2021, **27**(12), 730257.
- 8 X. H. Makhoba, C. Viegas Jr., R. A. Mosa, F. P. Viegas and O. J. Poole, *Drug Des., Dev. Ther.*, 2020, **14**, 3235–3249.
- 9 M. S. Brose, C. M. Nutting, B. Jarzab, R. Elisei, S. Siena, L. Bastholt, C. de la Fouchardiere, F. Pacini, R. Paschke, Y. K. Shong, S. I. Sherman, J. W. A. Smit, J. Chung, C. Kappeler, C. Peña, I. Molnár and M. J. Schlumberger, *Lancet*, 2014, **384**, 319–328.
- 10 A.-L. Cheng, Y.-K. Kang, Z. Chen, C.-J. Tsao, S. Qin, J. S. Kim, R. Luo, J. Feng, S. Ye, T.-S. Yang, J. Xu, Y. Sun, H. Liang, J. Liu, J. Wang, W. Y. Tak, H. Pan, K. Burock, J. Zou, D. Voliotis and Z. Guan, *Lancet Oncol.*, 2009, **10**, 25–34.

- 11 S. Wilhelm, C. Carter, M. Lynch, T. Lowinger, J. Dumas, R. A. Smith, B. Schwartz, R. Simantov and S. Kelley, *Nat. Rev. Drug Discovery*, 2006, **5**, 835–844.
- 12 S. M. Wilhelm, C. Carter, L. Tang, D. Wilkie, A. McNabola, H. Rong, C. Chen, X. Zhang, P. Vincent, M. McHugh, Y. Cao, J. Shujath, S. Gawlak, D. Eveleigh, B. Rowley, L. Liu, L. Adnane, M. Lynch, D. Auclair, I. Taylor, R. Gedrich, A. Voznesensky, B. Riedl, L. E. Post, G. Bollag and P. A. Trail, *Cancer Res.*, 2004, **64**, 7099–7109.
- 13 L. Zhong, Y. Li, L. Xiong, W. Wang, M. Wu, T. Yuan, W. Yang, C. Tian, Z. Miao, T. Wang and S. Yang, *Signal Transduction Targeted Ther.*, 2021, **6**, 201.
- 14 Y. S. Chang, J. Adnane, P. A. Trail, J. Levy, A. Henderson, D. Xue, E. Bortolon, M. Ichetovkin, C. Chen, A. McNabola, D. Wilkie, C. A. Carter, I. C. A. Taylor, M. Lynch and S. Wilhelm, *Cancer Chemother. Pharmacol.*, 2007, **59**, 561–574.
- 15 H. Geerts and L. Kennis, *Future Med. Chem.*, 2014, **6**, 1757–1769.
- 16 M. Agamennone, M. Fantacuzzi, S. Carradori, A. Petzer, J. P. Petzer, A. Angeli, C. T. Supuran and G. Luisi, *Molecules*, 2022, **27**, 7884.
- 17 G. E. Mathew, J. M. Oh, K. Mohan, M. V. Kumudhavalli, S. Jayanthi, H. Kim and B. Mathew, *Process Biochem.*, 2020, **99**, 246–253.
- 18 B. Mathew, S. C. Baek, D. G. Thomas Parambi, J. P. Lee, G. E. Mathew, S. Jayanthi, D. Vinod, C. Rapheal, V. Devikrishna, S. S. Kondarath, Md. S. Uddin and H. Kim, *Arch. Pharm.*, 2019, **352**(4), e1800309.
- 19 R. Sasidharan, B. H. Eom, J. H. Heo, J. E. Park, M. A. Abdelgawad, A. Musa, N. Gambacorta, O. Nicolotti, S. L. Manju, B. Mathew and H. Kim, *J. Enzyme Inhib. Med. Chem.*, 2021, **36**, 188–197.
- 20 J. M. Oh, T. M. Rangarajan, R. Chaudhary, R. P. Singh, M. Singh, R. P. Singh, A. R. Tondo, N. Gambacorta, O. Nicolotti, B. Mathew and H. Kim, *Molecules*, 2020, **25**, 2356.
- 21 A. Venkidath, J. M. Oh, S. Dev, E. Amin, S. P. Rasheed, A. Vengamthodi, N. Gambacorta, A. Khames, M. A. Abdelgawad, G. George, O. Nicolotti, H. Kim and B. Mathew, *Molecules*, 2021, **26**, 6004.
- 22 V. P. Vishal, J. M. Oh, A. Khames, M. A. Abdelgawad, A. S. Nair, L. R. Nath, N. Gambacorta, F. Ciriaco, O. Nicolotti, H. Kim and B. Mathew, *Pharmaceutics*, 2021, **13**, 850.
- 23 G. S. Jeong, S. Kaipakasseri, S. R. Lee, N. Marraiki, G. E. Batiha, S. Dev, A. Palakkathondi, F. S. Kavully, N. Gambacorta, O. Nicolotti, B. Mathew and H. Kim, *ChemMedChem*, 2020, **15**, 2257–2263.
- 24 C. T. Supuran, A. Scozzafava and A. Casini, *Med. Res. Rev.*, 2003, **23**, 146–189.
- 25 C. T. Supuran, *Nat. Rev. Drug Discovery*, 2008, **7**, 168–181.
- 26 C. T. Supuran, *Bioorg. Med. Chem. Lett.*, 2010, **20**, 3467–3474.
- 27 *Carbonic Anhydrase*, ed. C. T. Supuran, A. Scozzafava and J. Conway, CRC Press, 2004.
- 28 A. Bertucci, A. Moya, S. Tambutté, D. Allemand, C. T. Supuran and D. Zoccola, *Bioorg. Med. Chem.*, 2013, **21**, 1437–1450.
- 29 C. T. Supuran, *Future Med. Chem.*, 2011, **3**, 1165–1180.
- 30 S. Fossati, P. Giannoni, M. E. Solesio, S. L. Cocklin, E. Cabrera, J. Ghiso and A. Rostagno, *Neurobiol. Dis.*, 2016, **86**, 29–40.
- 31 C. T. Supuran, A. Scozzafava and A. Casini, *Med. Res. Rev.*, 2003, **23**, 146–189.
- 32 A. Innocenti, S. Beyza Öztürk Sarıkaya, İ. Gülçin and C. T. Supuran, *Bioorg. Med. Chem.*, 2010, **18**, 2159–2164.
- 33 C. Supuran, *Curr. Top. Med. Chem.*, 2007, **7**, 825–833.
- 34 C. T. Supuran, *Nat. Rev. Drug Discovery*, 2008, **7**, 168–181.
- 35 A. Guerri, F. Briganti, A. Scozzafava, C. T. Supuran and S. Mangani, *Biochemistry*, 2000, **39**, 12391–12397.
- 36 J. Lehtonen, B. Shen, M. Vihinen, A. Casini, A. Scozzafava, C. T. Supuran, A.-K. Parkkila, J. Saarnio, A. J. Kivelä, A. Waheed, W. S. Sly and S. Parkkila, *J. Biol. Chem.*, 2004, **279**, 2719–2727.
- 37 V. Alterio, A. Di Fiore, K. D'Ambrosio, C. T. Supuran and G. De Simone, *Chem. Rev.*, 2012, **112**, 4421–4468.
- 38 A. Maresca, C. Temperini, H. Vu, N. B. Pham, S.-A. Poulsen, A. Scozzafava, R. J. Quinn and C. T. Supuran, *J. Am. Chem. Soc.*, 2009, **131**, 3057–3062.
- 39 A. Scozzafava, T. Owa, A. Mastrolorenzo and C. Supuran, *Curr. Med. Chem.*, 2003, **10**, 925–953.
- 40 S. M. Monti, C. T. Supuran and G. De Simone, *Expert Opin. Ther. Pat.*, 2013, **23**, 737–749.
- 41 A. Bertucci, A. Moya, S. Tambutté, D. Allemand, C. T. Supuran and D. Zoccola, *Bioorg. Med. Chem.*, 2013, **21**, 1437–1450.
- 42 A. Thiry, J.-M. Dogne, C. Supuran and B. Masereel, *Curr. Top. Med. Chem.*, 2007, **7**, 855–864.
- 43 E. Berrino, B. Michelet, A. Martin-Mingot, F. Carta, C. T. Supuran and S. Thibaudeau, *Angew. Chem., Int. Ed.*, 2021, **60**, 23068–23082.
- 44 C. T. Supuran, *Bioorg. Med. Chem. Lett.*, 2023, **93**, 129411.
- 45 A. Nocentini and C. T. Supuran, *Expert Opin. Ther. Pat.*, 2018, **28**, 729–740.
- 46 J. Ghiso, S. Fossati and A. Rostagno, *J. Alzheimer's Dis.*, 2014, **42**, S167–S176.
- 47 S. Fossati, J. Cam, J. Meyerson, E. Mezhericher, I. A. Romero, P. O. Couraud, B. B. Weksler, J. Ghiso and A. Rostagno, *FASEB J.*, 2010, **24**, 229–241.
- 48 R. Parodi-Rullán, J. Ghiso, E. Cabrera, A. Rostagno and S. Fossati, *Aging Cell*, 2020, **19**(11), e13258.
- 49 S. Fossati, P. Giannoni, M. E. Solesio, S. L. Cocklin, E. Cabrera, J. Ghiso and A. Rostagno, *Neurobiol. Dis.*, 2016, **86**, 29–40.
- 50 M. K. Sun and D. L. Alkon, *J. Pharmacol. Exp. Ther.*, 2001, **297**, 961–967.
- 51 L. Canto de Souza, G. Provensi, D. Vullo, F. Carta, A. Scozzafava, A. Costa, S. D. Schmidt, M. B. Passani, C. T. Supuran and P. Blandina, *Neuropharmacology*, 2017, **118**, 148–156.
- 52 P. Blandina, G. Provensi, M. B. Passani, C. Capasso and C. T. Supuran, *J. Enzyme Inhib. Med. Chem.*, 2020, **35**, 1206–1214.
- 53 R. Ipe, J. M. Oh, S. Kumar, I. Ahmad, L. R. Nath, S. Bindra, H. Patel, K. Y. Kolachi, P. Prabhakaran, P. Gahtori, A. Syed, A. M. Elgorbanh, H. Kim and B. Mathew, *Mol. Diversity*, 2024, 1–17.

- 54 B. Mathew, J. M. Oh, D. G. T. Parambi, S. T. Sudevan, S. Kumar and H. Kim, Enzyme inhibition assays for monoamine oxidase, in *Neuroprotection*, ed. S. K. Ray, Methods in Molecular Biology, Humana, New York, 2024, vol. 2761, pp. 329–336.
- 55 B. Mathew, D. G. T. Parambi, G. E. Mathew, Md. S. Uddin, S. T. Inasu, H. Kim, A. Marathakam, M. K. Unnikrishnan and S. Carradori, *Arch. Pharm.*, 2019, **352**(11), e1900177.
- 56 M. B. H. Youdim, D. Edmondson and K. F. Tipton, *Nat. Rev. Neurosci.*, 2006, **7**, 295–309.
- 57 P. Riederer, L. Lachenmayer and G. Laux, *Curr. Med. Chem.*, 2004, **11**, 2033–2043.
- 58 N. Dinh Thanh, D. Son Hai, V. Ngoc Toan, H. Thi Kim Van, N. Thi Kim Giang and N. Minh Tri, *Arch. Pharm.*, 2024, **357**(5), e2300557.
- 59 N. A. Rehuman, A. G. Al-Sehemi, D. G. T. Parambi, T. M. Rangarajan, O. Nicolotti, H. Kim and B. Mathew, *ChemistrySelect*, 2021, **6**, 7162–7182.
- 60 G. Evtugyn, *Talanta*, 1998, **46**, 465–484.
- 61 Y. Miao, N. He and J.-J. Zhu, *Chem. Rev.*, 2010, **110**, 5216–5234.
- 62 S. Tian, X. Wang, L. Li, X. Zhang, Y. Li, F. Zhu, T. Hou and X. Zhen, *J. Chem. Inf. Model.*, 2017, **57**, 1474–1487.
- 63 Y.-G. Chen, *China Med. J.*, 2018, **131**, 1618–1624.
- 64 S. Kummar, H. X. Chen, J. Wright, S. Holbeck, M. D. Millin, J. Tomaszewski, J. Zweibel, J. Collins and J. H. Doroshov, *Nat. Rev. Drug Discovery*, 2010, **9**, 843–856.
- 65 R. Morphy and Z. Rankovic, *J. Med. Chem.*, 2005, **48**(21), 6523–6543.
- 66 X. Zhao, Q. Hu, X. Wang, C. Li, X. Chen, D. Zhao, Y. Qiu, H. Xu, J. Wang, L. Ren, N. Zhang, S. Li, P. Gong and Y. Hou, *Eur. J. Med. Chem.*, 2024, **279**, 116810.
- 67 S. Giovannuzzi, D. Chavarria, G. Provensi, M. Leri, M. Bucciantini, S. Carradori, A. Bonardi, P. Gratteri, F. Borges, A. Nocentini and C. T. Supuran, *J. Med. Chem.*, 2024, **67**, 4170–4193.
- 68 S. Carradori, M. Fantacuzzi, A. Ammazalorso, A. Angeli, B. De Filippis, S. Galati, A. Petzer, J. P. Petzer, G. Poli, T. Tuccinardi, M. Agamennone and C. T. Supuran, *Molecules*, 2022, **27**, 7816.
- 69 M. Şentürk, İ. Gülçin, Ş. Beydemir, Ö. İ. Küfrevioğlu and C. T. Supuran, *Chem. Biol. Drug Des.*, 2011, **77**, 494–499.
- 70 A. Innocenti, I. Gülçin, A. Scozzafava and C. T. Supuran, *Bioorg. Med. Chem. Lett.*, 2010, **20**, 5050–5053.
- 71 R. Florio, B. De Filippis, S. Veschi, V. di Giacomo, P. Lanuti, G. Catitti, D. Brocco, A. di Rienzo, A. Cataldi, I. Cacciatore, R. Amoroso, A. Cama and L. De Lellis, *Int. J. Mol. Sci.*, 2023, **24**, 1977.
- 72 M. Fantacuzzi, M. Gallorini, N. Gambacorta, A. Ammazalorso, Z. Aturki, M. Balaha, S. Carradori, L. Giampietro, C. Maccallini, A. Cataldi, O. Nicolotti, R. Amoroso and B. De Filippis, *Pharmaceuticals*, 2021, **14**, 984.
- 73 P. Di Fermo, S. Di Lodovico, R. Amoroso, B. De Filippis, S. D'Ercole, E. Di Campi, L. Cellini and M. Di Giulio, *Antibiotics*, 2020, **9**, 891.
- 74 E. S. Di Filippo, L. Giampietro, B. De Filippis, M. Balaha, V. Ferrone, M. Locatelli, T. Pietrangelo, A. Tartaglia, R. Amoroso and S. Fulle, *Molecules*, 2020, **25**, 5770.
- 75 I. Nishimori, D. Vullo, A. Innocenti, A. Scozzafava, A. Mastrolorenzo and C. T. Supuran, *J. Med. Chem.*, 2005, **48**, 7860–7866.
- 76 S. Carradori, M. Fantacuzzi, A. Ammazalorso, A. Angeli, B. De Filippis, S. Galati, A. Petzer, J. P. Petzer, G. Poli, T. Tuccinardi, M. Agamennone and C. T. Supuran, *Molecules*, 2022, **27**, 7816.
- 77 M. Agamennone, M. Fantacuzzi, S. Carradori, A. Petzer, J. P. Petzer, A. Angeli, C. T. Supuran and G. Luisi, *Molecules*, 2022, **27**, 7884.
- 78 R. G. Khalifah, *J. Biol. Chem.*, 1971, **246**, 2561–2573.
- 79 D. Pirollo, B. Righino, C. Camponeschi, F. Ria, G. Di Sante and M. C. De Rosa, *Sci. Rep.*, 2023, **13**, 1494.
- 80 M. Durgun, S. Akocak, N. Lolak, F. Topal, Ü. M. Koçyiğit, C. Türkeş, M. Işık and Ş. Beydemir, *Chem. Biodiversity*, 2024, **21**(2), e202301824.
- 81 A. Nocentini, A. Costa, A. Bonardi, A. Ammara, S. Giovannuzzi, A. Petreni, G. Bartolucci, B. Rani, M. Leri, M. Bucciantini, J. G. Fernández-Bolaños, Ó. López, M. B. Passani, G. Provensi, P. Gratteri and C. T. Supuran, *J. Med. Chem.*, 2024, **67**, 16873–16898.
- 82 C. Temperini, A. Scozzafava, D. Vullo and C. T. Supuran, *J. Med. Chem.*, 2006, **49**, 3019–3027.
- 83 M. R. Buemi, A. Di Fiore, L. De Luca, A. Angeli, F. Mancuso, S. Ferro, S. M. Monti, M. Buonanno, E. Russo, G. De Sarro, G. De Simone, C. T. Supuran and R. Gitto, *Eur. J. Med. Chem.*, 2019, **163**, 443–452.
- 84 A. Saxena, A. M. G. Redman, X. Jiang, O. Lockridge and B. P. Doctor, *Chem.-Biol. Interact.*, 1999, **119–120**, 61–69.
- 85 F. Nachon, E. Carletti, C. Ronco, M. Trovaslet, Y. Nicolet, L. Jean and P.-Y. Renard, *Biochem. J.*, 2013, **453**, 393–399.
- 86 E. Berrino, S. Carradori, F. Carta, F. Melfi, M. Gallorini, G. Poli, T. Tuccinardi, J. G. Fernández-Bolaños, Ó. López, J. P. Petzer, A. Petzer, P. Guglielmi, D. Secchi and C. T. Supuran, *Antioxidants*, 2023, **12**, 2044.
- 87 M. G. Kurban, R. Çakmak, E. Başaran, B. Türkmenoğlu and M. Şentürk, *J. Mol. Struct.*, 2024, **1314**, 138798.